Hindawi
Geofluids
Volume 2021, Article ID 2749373, 15 pages
https://doi.org/10.1155/2021/2749373

*Research Article*

# Optimization of Barrier Pillar Design in Longwall Mining with Top Coal Caving in Spontaneous Combustion Coal Seam

**Qiang Fu**,[1,2] **Ke Yang**,[1,3] **Qinjie Liu**,[1,2] **Shuai Liu**,[1,2] **Xiang He**,[1,2] **and Xin Lyu**[1,2]

[1]*State Key Laboratory of Mining Response and Disaster Prevention and Control in Deep Coal Mines, Anhui University of Science and Technology, Huainan 232001, China*
[2]*School of Mining Engineering, Anhui University of Science and Technology, Huainan 232001, China*
[3]*Institute of Energy, Hefei Comprehensive National Science Center, Hefei 230031, China*

Correspondence should be addressed to Ke Yang; keyang2003@163.com

Received 1 September 2021; Revised 28 September 2021; Accepted 4 October 2021; Published 31 October 2021

Academic Editor: Liang Xin



Determining a reasonable barrier pillar along gob-side entry of spontaneous combustion coal seam is of great significance to the prevention of spontaneous combustion. In this paper, considering the actual situation of 4301 and 4302 working faces of II-class spontaneous combustion coal seam in Changheng Mine, the characteristics of rock mass collapse and mining-induced stress redistribution of barrier pillar and adjacent area were analyzed, the cusp catastrophe model of coal pillar instability and the theoretical model of limit width of coal pillar air leakage spontaneous combustion were established, and a measurement scheme of side abutment pressure in 4301 working face was carried out. The theoretical model of the coal pillar along the gob-side entry shows that its instability is related to density of overlying strata, physical and mechanical parameters of coal body, dip angle of coal seam and weak face, and buried depth and mining width of working face. And the coal pillar in 4302 working face will be unstable if the width $a \leq 6.8$ m. Field measured data shows that 2-8 m is the stress-relaxation area of side solid coal. Then, the width of coal pillar was determined as 7 m. The maximum displacement of rib-to-rib and roof-to-floor of 4302 tailentry was 520 mm and 280 mm, respectively. The coal spontaneous combustion (CSC) observation monitoring results showed that the carbon monoxide volume fraction was in the normal range during the entire process of mining, and no other signs of gas were found. The research results can provide a reference for the barrier pillar designing in the mines under similar conditions.

## 1. Introduction

China is the world's largest producer and consumer of coal, accounting for more than 56.8% of its primary energy consumption. Thick coal seams are abundant in coal resources, accounting for 45% of the workable coal seam in China [1]. Longwall top coal caving (LTCC) and large mining height fully mechanized mining are the main ways to recover thick coal seam. However, CSC fires have always affected the safety and efficiency of mining production and lives of coal miners; it is one of the main disasters in coal mines [2]. Gob is the most prone location of CSC in coal mine, and 60% of CSC fires occur in gob [3]. In the process of longwall mining, the working faces in the mine are usually separated by barrier pillar. Entries are arranged on both sides of the barrier pillar to serve the production of working faces. According to the demand of coal mining, the barrier pillar usually has three functions: (1) isolating the working face, (2) protecting the entry and controlling the surface subsidence, and (3) protecting the next working face from the influence of ponding, residual gas, and roof collapse in the gob [4]. The width of the barrier pillar determines the position of the mining entry of the next working face to be mined and affects the ground pressure behavior on the gob-side entry. According to the width of barrier pillar, the entry layout in longwall mining can be divided into gob-side entry retained, entry protection with large coal pillar, and gob-side entry with narrow coal pillar [5, 6]. In the gob-side entry retaining, it is necessary to carry out roadside filling or roof cutting and the operation process is complex.

When the entry is affected by secondary mining, the surrounding rock deformation and damage is serious, and the later maintenance cost is high. In the entry protection with large coal pillar, the width of coal pillar is generally 15-50 m, which seriously wastes resources for thick coal seams and is not conducive to improving the resource recovery rate. The gob-side entry with narrow coal pillar is generally provided with 3-15 m coal pillar along the edge of the gob. This arrangement avoids the entry without filling body from being in the peak area of side abutment pressure, which makes the entry easy to maintain and conducive to popularization.

The design of barrier pillar is extremely important for the successful and effective operation of coal mining. Its main purpose is to make the barrier pillar meet the functional requirements of the above three aspects under the influence of mining-induced stress. Unreasonable design of barrier pillar will lead to roof fall, rib spalling, deformation, and failure of support structure, even coal burst and CSC. On the determination of the width of barrier pillar, many scholars and engineers have carried out a lot of research by means of field measurement, statistics, theoretical calculation, and numerical simulation and put forward lots of effective design methods. In recent years, a series of research on the stress and yield behavior of the coal pillar has been studied, including the study methods, the formula to calculate the reasonable width of the coal pillar, and the control mechanism of the surrounding rock [7, 8]. Based on the field stress measurement data and statistical analysis, Bieniawski [9] established the empirical relationship between the in situ strength of coal and the size of coal pillar, and Salamon and Munro [10] established barrier pillar sample banks in some mine areas in South Africa. The empirical equation related to coal pillar strength and its aspect ratio is proposed by means of comparative analysis and stability statistics and corrected through industrial tests. Using similar methods, a large number of sample statistics are carried out for coal mines in Australia, and similar strength empirical formulas are also obtained [11]. Based on the field survey data of American coal mines and comprehensively considering the influence of complete rock strength and discontinuity on coal pillar strength, an evaluation method of barrier pillar strength is proposed [12]. Chen et al. [13] proposed a design method for strip coal pillar in East China by estimating surface subsidence and successfully conducted industrial tests. Yu et al. [14] monitored the stress and deformation of the coal pillar in the longwall face of soft stratum in Tashan Mine, China, and determined the optimal width of the barrier pillar. Taking the Zhaogu No. 2 Mine in Xinxiang City, China, as the engineering background, Jiang et al. [15] considered the weakening effect of fracture development on the rigidity of the rock mass and proposed a tension weakening model to analyze the stability of the barrier pillar.

Numerical simulation is a convenient method that can effectively analyze various influencing factors. In recent years, it has been widely used by scholars to determine the width of barrier pillar. Zhou et al. [16] used FLAC3D software to simulate the instability behavior of coal pillar under the superposition of static load and dynamic load and obtained the dynamic response and instability mechanism of barrier pillar. Zhang et al. [17] proposed to use the double-yield model to simulate gob materials, and obtain a more real simulation process through parameter correction to analyze the stability of stope pillars in underground coal mines. Xu et al. [18] studied the width of coal pillar along the gob-side entry in the isolated working face of the soft coal seam through numerical simulation and monitored the stability of the surrounding rock of the entry with a small coal pillar of 5 m. Based on filed monitoring data combined with discontinuous numerical simulation software, Wu et al. [19] simulated the deformation and stress distribution of coal pillar in inclined rock strata under the influence of multiple mining operations.

The above studies mostly discussed the influence of side abutment pressure distribution, resource recovery rate, and the stability of coal pillar and entry on the reserved width of barrier pillar from the perspective of rock mechanics. For the spontaneous combustion thick coal seam with bursting liability, in addition to ensuring the stability of adjacent entries, the barrier pillar is mainly used to isolate the gob to control the air leakage of coal pillar. A reasonable coal pillar size has a preventive effect on coal pillar spontaneous combustion [20, 21]. Therefore, in order to determine the reasonable width of the coal pillar when the narrow coal pillar is selected to drive along the gob to isolate the gob, it is also necessary to consider the sudden instability (coal burst) of the coal pillar under high-intensity mining, as well as the air leakage and spontaneous combustion of the coal pillar caused by supporting pressure. Based on the engineering background of narrow barrier pillar in LTCC working face of II-level spontaneous combustion coal seam, using the comprehensive research methods of mechanical modeling and field measurement, this paper discusses the determination method of the optimal narrow coal pillar width to prevent sudden instability and spontaneous combustion of coal pillar. The research results can provide reference for the design of barrier pillar in coal face under similar conditions.

## 2. Engineering Background

The selected mine with typical geological conditions is Changheng Mine in Lvliang mine area, Shanxi Province, China. The geographical location is shown in Figure 1. The main coal seams of Changheng Mine are No. 4 coal and No. 9 coal. The burial depth of No. 9 coal is about 360 m, and the average thickness is 9.46 m. At present, it is still in the stage of preparation for mining. The buried depth of No. 4 coal is relatively shallow, about 280 m, and the thickness of coal seam is 5.8-9.2 m, with an average of 8.2 m. The LTCC is adopted. The mechanical mining height is 3.0 m, the coal caving height is about 5.2 m, and the coal seam dip angle is 5°. It is mainly dark coal, which is a high-quality coking coal blending and coal chemical raw material. At present, 4301 working face in the third district of No. 4 coal seam is being mined, with stable coal seam occurrence and simple structure. The 4301 working face is located at the western boundary of the third mining district, adjacent to the 4302 working face in the east and the 43

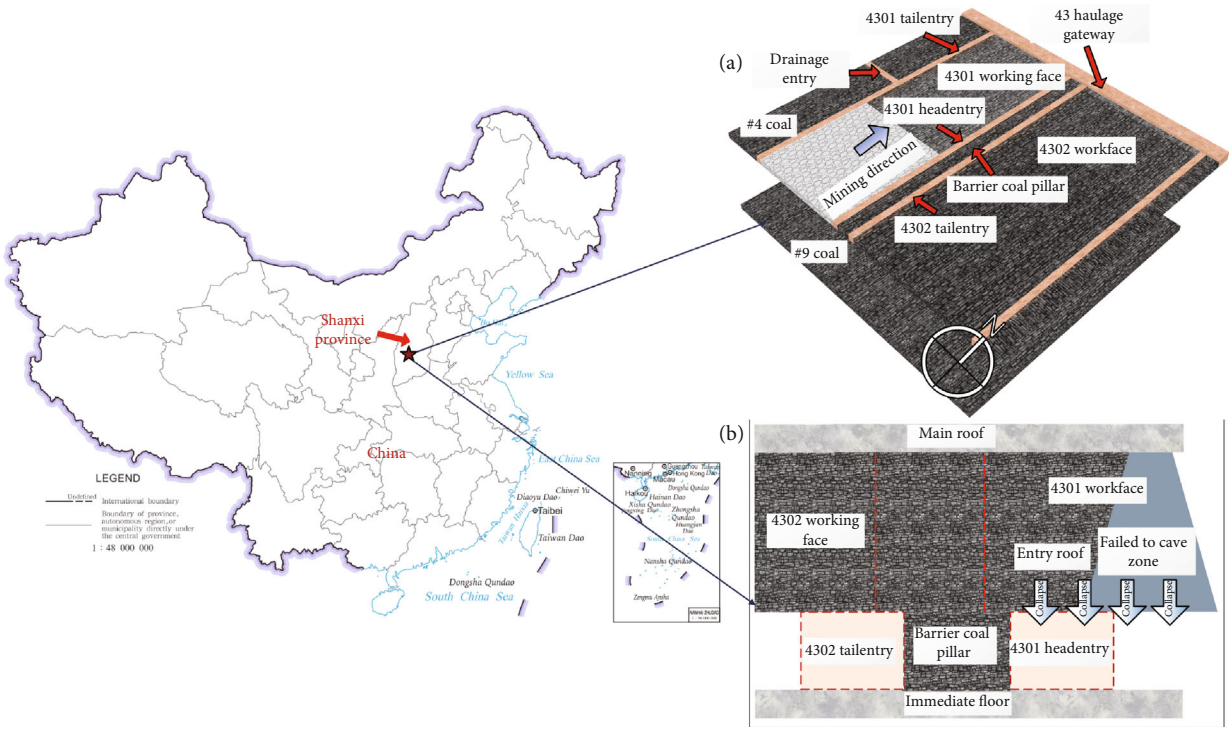


Figure 1: Mining conditions of Changheng Mine.

haulage gateway in the north. The inclined width of the working face is 214 m, and the strike length is 1550 m. The working faces of other mining district in No. 4 coal were threatened by ground pressure, and the width of the barrier pillars is 50 m, which is a serious waste of resources and large economic losses. Therefore, during the design and excavation of tailentry in 4302 working face, it is the first time to explore the retention of narrow coal pillar as the barrier between working faces. The spatial positions of the two working faces are shown in Figure 1(a).

The immediate roof of No. 4 coal is medium sandstone, with an average thickness of 4.9 m and a Protodyakonov coefficient of $f = 3.1$. The main roof is fine sandstone, with an average thickness of 18.5 m, intercalated with a thin layer of medium sandstone and non-minable coal seam, with a Protodyakonov coefficient of $f = 4.2$. The immediate floor is coarse sandstone with an average thickness of 6.8 m, and the old bottom is siltstone with an average thickness of 18.25 m. The roof and floor of No. 4 coal are medium stable strata with good mining conditions. However, the strength of the roof is relatively high, and the first and periodic weighting intervals of the working face are relatively large, which will cause high stress concentration during the mining process, and it is easy to induce the pressure bump. The Protodyakonov coefficient is $f = 2.9$ of No. 4 coal. During the periodic weighting from the working face, the ejection of broken coal often occurs at the place 12-14 m ahead of the entries. In serious cases, coal burst accidents occur, which greatly threatens the equipment safety and lives of miners. There was an accident of spontaneous combustion in gob before working face in No. 4 coal. The gas chromatography oxygen absorption identification method was used to identify the spontaneous combustion tendency of No. 4 coal. The test results show that the physical oxygen absorption of No. 4 coal is 0.59 $cm^3/g$, belonging to II-class spontaneous combustion coal seam. Therefore, in the design of narrow coal pillar along the gob, the influence of strong ground pressure behavior and coal seam spontaneous combustion must be considered at the same time.

## 3. Theoretical Analyses

*3.1. Characteristics of Rock Mass Collapse and Stress Redistribution.* After the mining of the working face is completed, the mining-induced stress is concentrated on the suspended roof and the exposed coal around the gob. The fracture and migration of overlying strata and the destruction of surrounding shallow coal bodies lead to the mining-induced stress redistribution of surrounding rock in gob. This paper mainly studies how to design narrow coal pillar so that it can still meet the production demand under the action of abutment pressure, so it only pays attention to the side abutment pressure in gob. The evolution of side abutment pressure is closely related to coal seam thickness, roof and floor structural characteristics, coal and rock mass strength, and coal mining method [22, 23]. For LTCC, the head areas at both ends of the working face are important exits integrating mining, transportation, ventilation, and pedestrians. In order to ensure the safety of this area, most working faces of LTCC adopt the method of no or less coal caving in the head areas at both ends. However, with the advance of the working face, the face-end support and transition support move forward, and the top coal and entry roof not placed in the head area will lose support and will collapse to the entry under the action of ground pressure, as

shown in Figure 1(b). In order to obtain the characteristics of the caving zone at the end of LTCC working face, Zhang et al. [24] drilled holes in Baodian Mine in China and obtained the image of the collapse state of coal and rock mass in the gob for the first time. This study also proves that the top coal and roof caving in the end area are progressive failure, and the side abutment pressure will change with this progressive failure.

After the LTCC working face advanced, the immediate roof and main roof collapse to the gob successively. At the same time, due to the forward movement of the face-end support, part of the noncaving coal at the end collapses and forms a slope with a natural rest angle of $\alpha$. After the main roof collapses, the load of the overlying strata is transferred to the boundary coal pillar, forming the side abutment pressure, as shown in Figure 2(a). This pressure usually forms stress-relaxation area (plastic failure area) A, stress-concentration area B, and primary rock stress area C near the coal pillar. The peak position of abutment pressure is close to the headentry at this moment.

The collapse of coal and rock mass at the top of the end area is gradual. As the face advances, the undergoing rotary deformation of the key rock blocks of main roof occurs. The top coal ① (C①) and immediate roof ① (R①) of the face-end support collapse and naturally accumulated to form a collapsed shape as shown in Figure 2(b). After C① and R① collapsed, the side abutment pressure in the coal pillar began to transfer to the deep of solid coal. Stress-relaxation area (plastic failure area) A, stress-concentration area B expanded, and the peak stress decreased.

After the coal seam was mined out, the roof of gob boundary will maintain its own stability for a certain period of time. However, with the continuous advancement of the working face, the rotation and subsidence of main roof key blocks will continue. The roof of headentry will continue to be unstable. Thus, under the action of main roof rotation, top coal ② (C②) and immediate roof (R②) collapse and accumulate in the form shown in Figure 2(c). The self-weight of the main roof key blocks and the load of overlying strata all act on the shallow area of the coal pillar and the accumulated gangue. Then, the side abutment pressure in the coal pillar (area B) is greatly transferred to the deep part of the solid coal, and the range of plastic area A is rapidly expanded. However, the peak stress is further reduced compared with the previous one.

Figure 2 shows the gradual collapse process of the top coal and rock mass in the face-end area and its effect on the side abutment pressure in the coal pillar after top-coal caving. The analysis shows that when the rotation of the main roof key blocks tends to be stable, there is a large area affected by side abutment pressure in the boundary pillar of the gob. From the perspective of preventing coal burst, the entry of next working face can only be layout in area A or C. For the gob-side entry with a narrow coal pillar, it can only be arranged in area A.

For spontaneous combustion coal seam, the fundamental principle of developing gob-side entry with a narrow coal pillar is to arrange the entry in the stress-relaxation area in the solid coal near gob to reduce the sudden instability of coal pillar (coal burst). Furthermore, it is required that the coal pillar still has self-supporting capacity. If the coal pillar is completely crushed, it is very easy to cause air leakage and spontaneous combustion of the coal pillar. Based on the above two considerations, the corresponding theoretical calculation models are explored, respectively, which provides a reference for the design of entry layout.

*3.2. Cusp Catastrophe Model for Sudden Instability of Coal Pillar.* The elastoplastic analysis of coal pillar is mainly to judge its state by comparing the internal stress of rock mass with the tensile or shear strength of rock mass itself, which cannot reflect the severity of failure. The pillar collapse initiates suddenly in bursting liability coal seam. The catastrophe theory can well solve this kind of problem in the study of coal rock fracture instability. The determination of critical surface is the core of catastrophe theory, and cusp catastrophe theory is widely used because of its simple critical surface structure, strong geometric intuition, and easy to understand. The general research idea is to establish the cusp catastrophe model and find out the expression of the standard potential function and obtain the bifurcation point set equation through a series of mathematical calculations. If the control variables meet the bifurcation point set equation, the system will catastrophize. We can find out the conditions that should be met for the sudden change of the system. Based on the cusp catastrophe theory, the mechanical criterion of static failure forms such as spalling of barrier pillar is explored [25], but the elastic-plastic analysis is more suitable for local nonimpact failure. The authors believe that the cusp catastrophe model can provide reference for analyzing the systematic collapse initiates suddenly in bursting liability coal seam. The cusp catastrophe model is shown in Figure 3.

It can be seen from Figure 3 that there are three regions, namely, the upper lobe, the middle lobe, and the lower lobe, in the balance surface. In this model, the upper lobe is the stable state of the isolated coal pillar, the lower lobe is the instability and destruction state of the coal pillar, and the middle lobe is the sudden change area of the state. When the variable that controls the instability of the barrier pillar changes, the state variable is prompted to change accordingly. When the state variable changes along the path A shown in Figure 3, the control variable satisfies the change process of the branch point set equation. Then, the path intersects the set of divergent points, and the system undergoes a sudden change. In this model, it means that the barrier pillar has sudden instability.

The theory of stable core area shows that under the action of overlying load $P$, plastic failure area is formed on both sides of coal pillar, and there should be a certain range of elastic core area in the middle to maintain stability. There are a large number of structural weak planes with different scales in the plastic failure area of coal pillar. Assuming that the displacement of coal pillar under the action of overlying load is $v$, the shear stress on each structural weak plane $\tau_s$ can be expressed as follows:

$$\tau_s = G_s \frac{v}{D_s} \exp\left(-\frac{v}{v_0}\right), \tag{1}$$

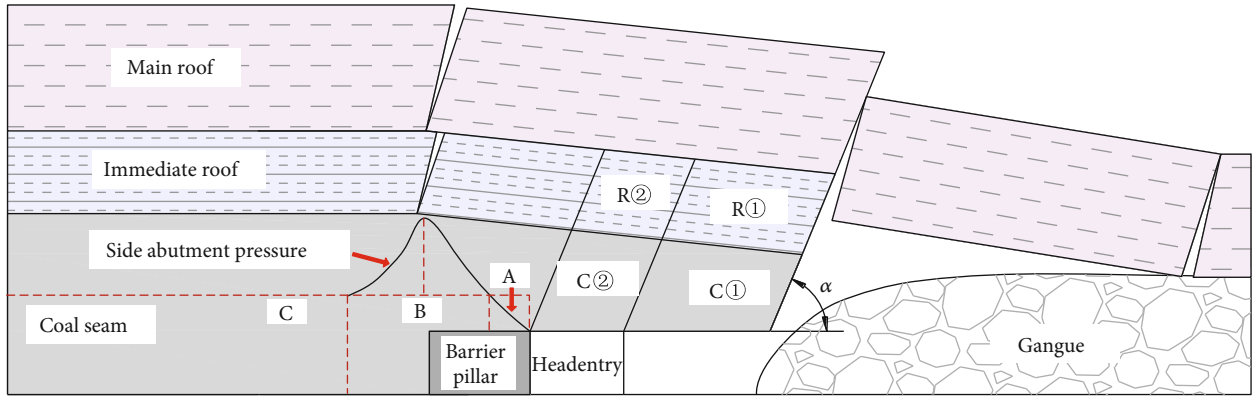


(a) The main roof begins to collapse

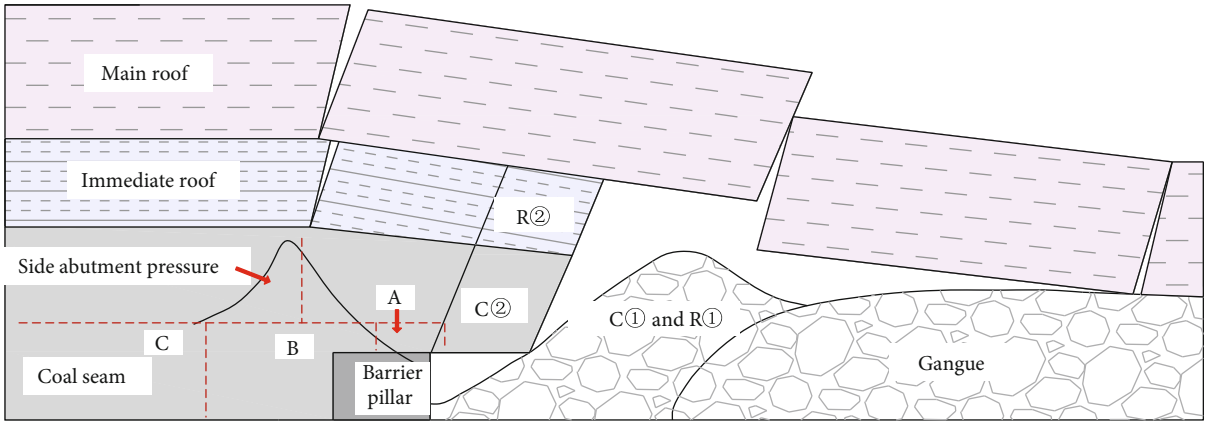


(b) The top coal and immediate roof of face-end support collapse

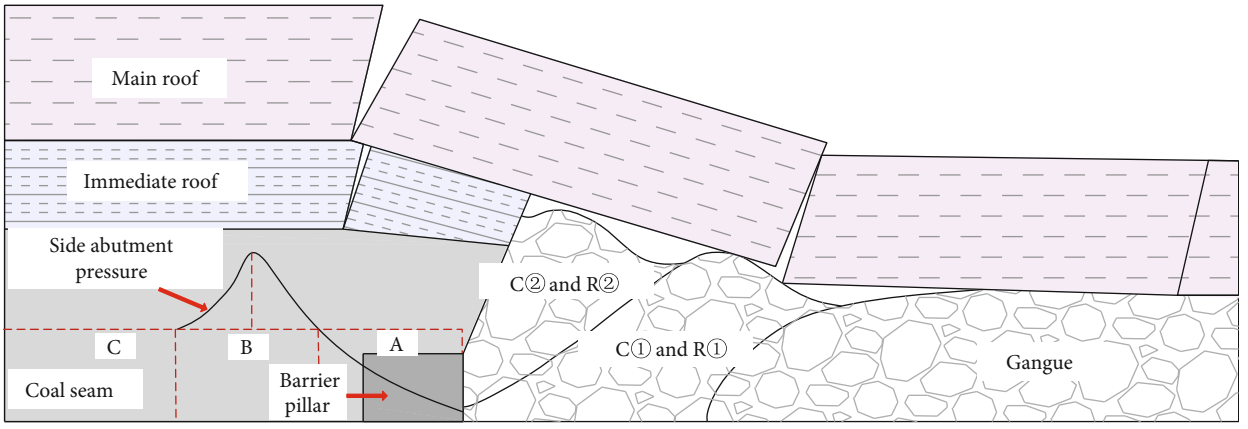


(c) The top coal and immediate roof of headentry collapse

Figure 2: Collapse process of coal and rock mass and evolution of side abutment pressure in face-end area.

where $G_s$ is the shear modulus of rock mass in plastic failure area, $D_s$ is the thickness of weak surface of structure in plastic failure area, and $v_0$ is the peak stress displacement.

In the stable elastic core area, the shear stress on the weak plane of the structure is presented as follows:

$$\tau_e = G_e \frac{v}{D_e}, \tag{2}$$

where $G_e$ is the shear modulus of rock mass in elastic core area and $D_e$ is the thickness of the weak surface of the structure in the elastic core region.

Under the condition of displacement of coal pillar is $v_0$ and displacement of structural weak plane is $v$, the potential energy of structural weak plane in section coal pillar in plastic failure area and elastic core area is, respectively, presented as follows:

$$V_s = \frac{1}{2}\tau_s \frac{v}{D_s} D_s l_s = \frac{G_s l_s v^2}{2D_s} e^{-v/v_0}, \tag{3}$$

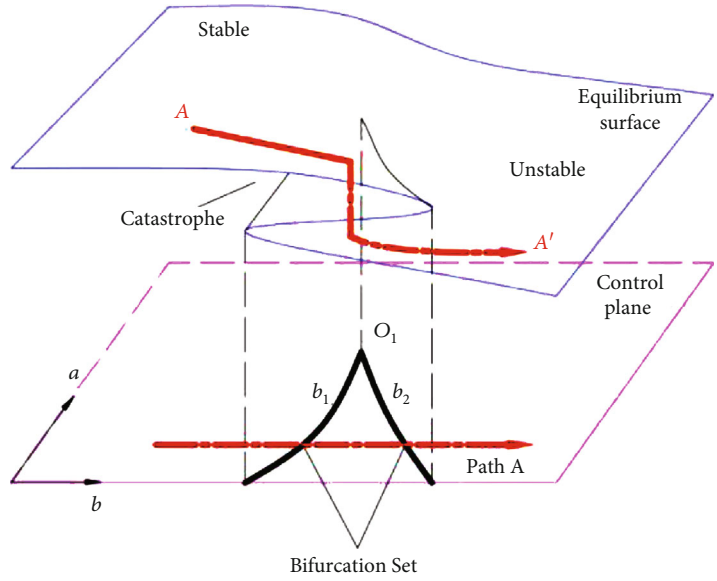


Figure 3: Cusp catastrophe model of coal pillar.

$$V_e = \frac{1}{2}\tau_e \frac{v}{D_e} D_e l_e = \frac{G_e l_e v^2}{2D_e}. \tag{4}$$

In Equations (3) and (4), $l_s$ is the length of slip surface in plastic failure area and $l_e$ is the length of slip surface in elastic core region. Then, the total potential energy of the coal pillar system is presented as follows:

$$V = V_s + V_e + V_P = \frac{G_s l_s v^2}{2D_s} e^{-v/v_0} + \frac{G_e l_e v^2}{2D_e} + Pv \sin(\partial + \theta), \tag{5}$$

where $\partial$ is the dip angle of coal seam and $\theta$ is the dip angle of structural weak plane. Assuming that the width of the barrier pillar is $a$, the width of the adjacent ready mining face is $b$, and the buried depth of the coal seam is $H$, the expression of the overlying load is presented as follows:

$$P = \gamma H\left[a + \frac{b}{2}\left(2 - \frac{b}{0.6H}\right)\right]. \tag{6}$$

Then, Equation (5) can be expressed as follows:

$$V = V_s + V_e + V_P = \frac{G_s l_s v^2}{2D_s} e^{-v/v_0} + \frac{G_e l_e v^2}{2D_e} + \gamma H v\left[a + \frac{b}{2}\left(2 - \frac{b}{0.6H}\right)\right] \sin(\partial + \theta). \tag{7}$$

Find the first derivative of Equation (7) to obtain the equilibrium surface equation as follows:

$$V' = V_s' + V_e' + V_P' = \frac{G_s l_s v}{D_s} e^{-v/v_0} + \frac{G_e l_e v}{D_e} - \gamma H\left[a + \frac{b}{2}\left(2 - \frac{b}{0.6H}\right)\right] \sin(\partial + \theta) = 0. \tag{8}$$

Based on the basic expression of cusp catastrophe model, Taylor expansion of Equation (8) is required. Expand at $v = v_1 = 2v_0$ to get the following:

$$V' = \frac{2}{3}\frac{G_s l_s v_1 e^{-2}}{D_s}\left[\left(\frac{v - v_1}{v_1}\right)^3 + \frac{3}{2}\left(\frac{G_e l_e e^2}{G_s l_s} - 1\right)\left(\frac{v - v_1}{v_1}\right) + \frac{3}{2}\left(1 + \frac{G_e l_e e^2}{G_s l_s} - \gamma H\left(a + \frac{b}{2}\left(2 - \frac{b}{0.6H}\right)\right)\right)\frac{D_s e^2 \sin(\partial + \theta)}{G_s l_s v_1}\right] = 0. \tag{9}$$

In order to change Equation (9) into the standard form of cusp mutation, let:

$$x = \frac{v - v_1}{v_1}, \tag{10}$$

$$P = \frac{3}{2}\left(\frac{l_e G_e e^2}{l_s G_s} - 1\right), \tag{11}$$

$$q = \frac{3}{2}\left[1 + \frac{l_e G_e}{l_s G_s} - \frac{\gamma H D_s e^2 \sin(\partial + \theta)}{G_s l_s v_1}\left(a + \frac{b}{2}\left(2 - \frac{b}{0.6H}\right)\right)\right]. \tag{12}$$

The standard form of cusp catastrophe model with state variable $x$ and control variables $p$ and $q$ can be obtained from Equations (9), (10), (11), and (12):

$$x^3 + px + q = 0. \tag{13}$$

According to the cusp catastrophe theory, the bifurcation point set equation is presented follows:

$$8p^3 + 27q^2 = 0. \tag{14}$$

The criteria for sudden destabilization conditions of

barrier pillars are obtained from Equations (11) and (12) brought in Equation (14):

$$2\left(\frac{l_e G_e e^2}{l_s G_s} - 1\right)^3 + 9\left[1 + \frac{l_e G_e}{l_s G_s} - \frac{\gamma H D_s e^2 \sin(\partial + \theta)}{G_s l_s v_1}\left(a + \frac{b}{2}\left(2 - \frac{b}{0.6H}\right)\right)\right]^2 \le 0. \quad (15)$$

*3.3. Limit Width Model of Coal Pillar Spontaneous Combustion.* For spontaneous coal seams, the spontaneous combustion of coal pillar is caused by the destruction of coal pillar under the action of roof load, forming through cracks and causing air leakage on both sides of the coal pillar, making the coal seams exposed to oxygen for a long time. After the formation of narrow coal pillar, coal body changes from three-way compression to two-way compression, and primary cracks are easier to expand and penetrate. Under the negative pressure of ventilation, air leakage occurs on both sides of the coal pillar. Under the action of negative ventilation pressure, air leakage occurs on both sides of the coal pillar. When the air leakage meets the conditions of ventilation, oxygen supply, and heat storage at the same time, spontaneous combustion of coal pillar is a high probability event. The key to control the spontaneous combustion of narrow coal pillar is whether the coal pillar can effectively isolate the air leakage between entry and gob.

Air leakage in coal pillar can be approximately considered to comply with Darcy's law of seepage, and then

$$V = \frac{K}{\mu}\frac{\partial p}{\partial l}, \quad (16)$$

where $V$ is the seepage velocity of air leakage through coal pillar, m/s. $K$ is the permeability of coal pillar, $m^2$. $\mu$ is the dynamic viscosity of air flow, generally $0.18 \times 10^5$Pa · s. $\partial p/\partial l$ is the air leakage pressure gradient, Pa/m.

The permeability of coal pillar is related to the width-to-height ratio of coal pillar, as well as the stress state and stress path. Laboratory experiments show that the permeability of briquette and pore-developed coal samples decreases first and then increases as the stress increases [26], as shown in Figure 4(a). The field measurement of coal body permeability shows that with the decrease of the distance between the working face and the observation point, the permeability of the coal increases gradually from the fixed value due to mining, decreases slightly before approaching the peak stress, and then increases rapidly due to the coal entering the elastic-plastic or plastic state at the observation point. The permeability of the coal in the whole stress process is higher than the original permeability [27, 28], as shown in Figure 4(b). After the coal body is affected by the front abutment pressure, the permeability is about 3-6 times of the original permeability.

After the coal body is compressed and loosened, the air leakage wind speed that is easy to cause spontaneous combustion is 0.1-0.24 m/min, and the limit wind speed that will not cause spontaneous combustion is less than 0.02-0.05 m/min [29]. The wider the reserved coal pillar, the higher the reliability of preventing air leakage. If the wind speed of air leakage is controlled below 0.02 m/min, the coal pillar will not induce spontaneous combustion due to compressed crushing and air leakage. The width of the coal pillar shall have the condition of Equation (17), where the air leakage pressure difference on both sides of the coal pillar is shown.

$$L \ge 60\frac{K}{\mu} \cdot \frac{\Delta P}{0.02}. \quad (17)$$

## 4. Field Measurement Scheme

*4.1. Field Measurement Scheme of Side Abutment Pressure.* Field measurement is one of the most direct, accurate, and reliable means to study engineering problems. The theoretical analysis points out that for coal seam threatened by strong ground pressure, when the narrow coal pillar is designed to drive along the gob, the entry and coal pillar can only be arranged in the stress-relaxation area A. The change of side abutment pressure with the advance of the working face and the final stable state can be monitored on site by embedding a borehole stress meter in the coal pillar in advance. Most of the existing measured studies on side abutment pressure are to drill holes directly into the lateral coal body at the headentry or tailentry of the working face. Due to the difficulty of drilling construction and easy to collapse, the drilling depth generally does not exceed 20 m. For the working face of deep well or thick coal seam, the influence range of side abutment pressure can reach 50-130 m [30]. It is impossible to fully grasp the distribution characteristics of side abutment pressure with traditional stress monitoring methods.

Considering the above factors, the influence range of side abutment pressure is monitored by referring to the lateral abutment pressure monitoring scheme implemented by Wang et al. [31] in Zhaolou Mine, China. In this monitoring scheme, the borehole stress meter is arranged at 4301 drainage entry vertically connected with the 4301 tailentry. The drainage entry is about 90 m long and located in the boundary coal pillar of 43 districts, as shown in Figure 1(a). When the working face passes through the 4301 drainage entry, the gob can be isolated by roadside backfilling body, and the live monitoring equipment in the drainage entry can continue to operate, ensuring the continuity of monitoring. If monitoring equipment is arranged in the mining entry, according to the requirements of relevant technical specifications for coal mine safety production in China, live equipment is not allowed to operate in the gob and must be removed

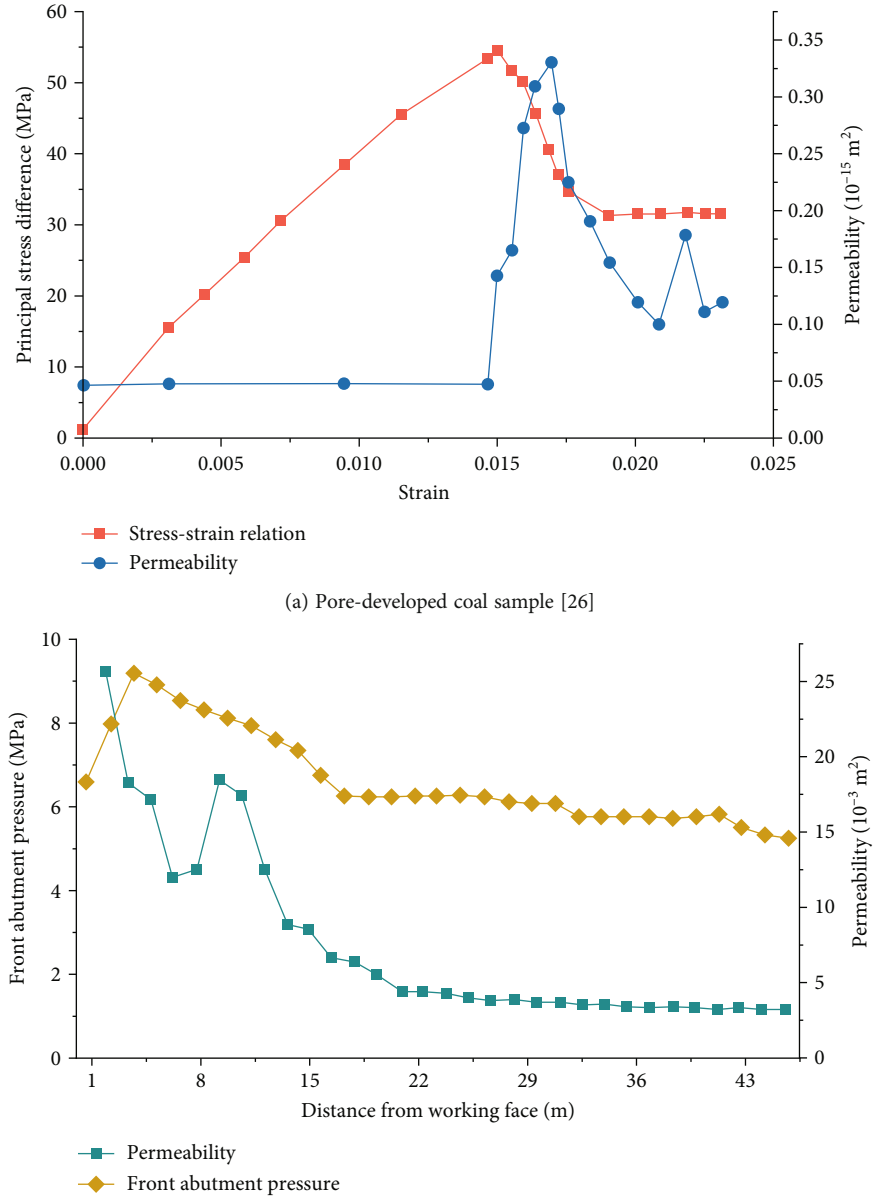


(a) Pore-developed coal sample [26]

(b) Intact coal body [27]

Figure 4: Variation curve of coal permeability.

when the working face is advanced to the monitoring equipment [32].

Firstly, drill holes with a depth of 20 m are successively arranged in the 4301 drainage entry. The depth of 20 m is selected to reduce the interference of the stress redistribution of the surrounding rock of the drainage entry on the stress meter of the coal body and to ensure the smooth construction of the site. A total of eight borehole stress meters are arranged in the 4301 drainage entry, and the spacing is shown in Figure 5. The farthest stress meter is 50 m away from 4301 tailentry. The installation height of borehole stress gauge is 1.5 m. By connecting the self-made single 1.5 m long hollow metal rod in turn, push the stress meter into the bottom of the borehole. Then, the portable hydraulic pump is used to inject liquid into the stress meter, and the pressure is maintained at 5.5 MPa to make the stress meter closely fit with the coal wall of the borehole. The stress meter and related auxiliary installation tools are shown in Figure 6. After the hydraulic pump is removed, a pressure monitor is installed at the outer port of the stress meter, which can wirelessly receive and send data. The single transmission range is 0-50 m, and the real-time data of monitoring hole pressure is sent every 3 minutes. Next, install the data transmission system. The data of each pressure monitor is wirelessly transmitted to the pressure monitoring station in the drainage entry, and the monitoring station is connected with the optical transceiver through optical fiber. The optical transceiver is an underground data storage station, which

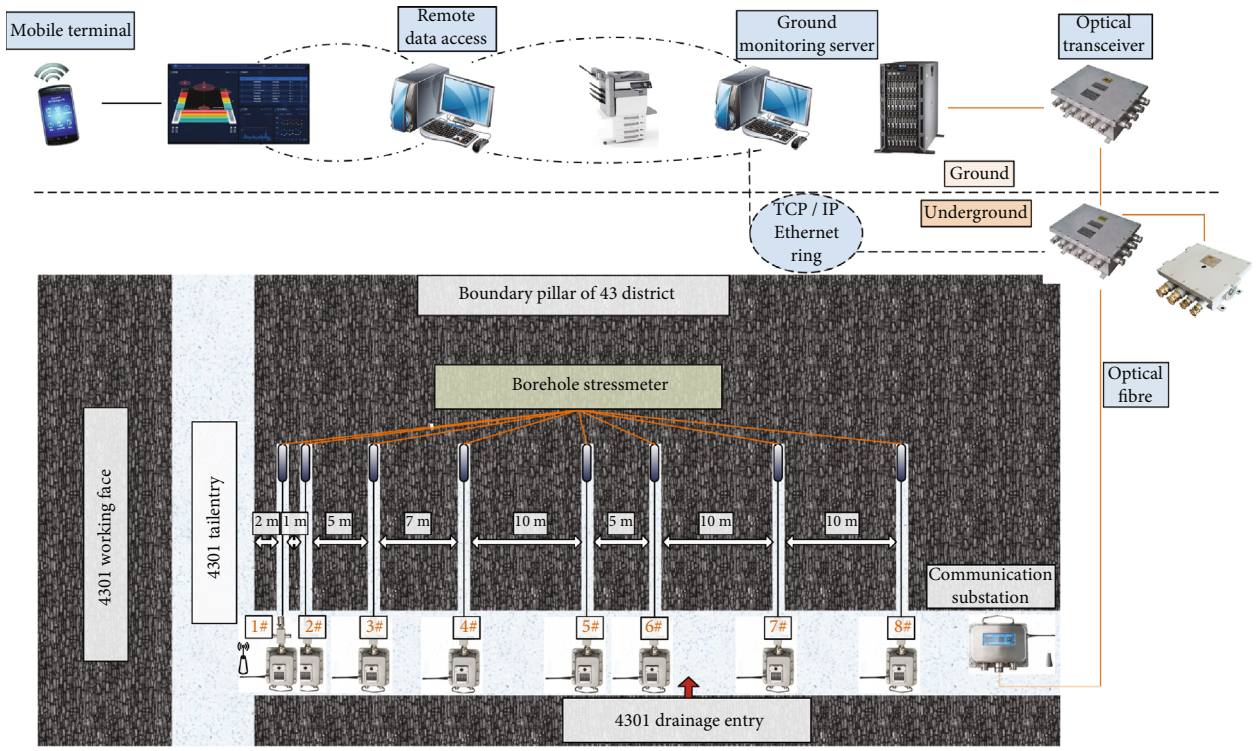


Figure 5: Layout plan of borehole stress meter.

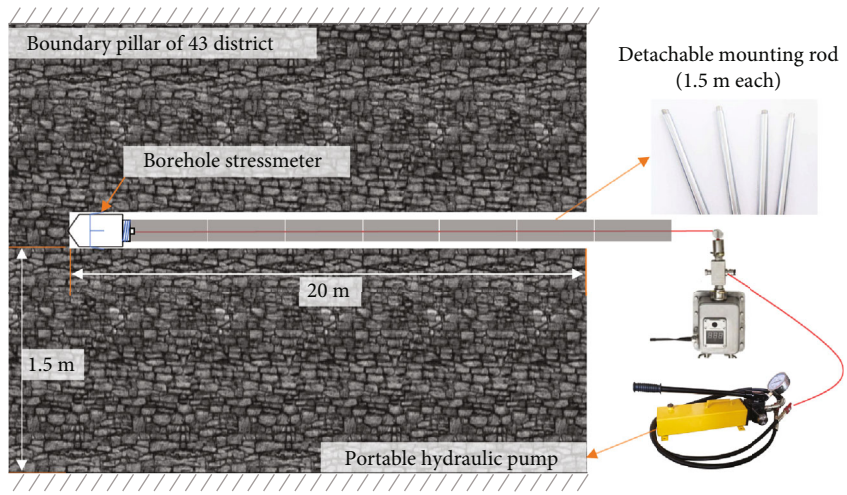


Figure 6: Installation of borehole stress meter.

can receive a variety of monitoring system data at the same time. The underground optical transceiver can transmit data to the ground in real time through the original TCP/IP Ethernet ring network or optical fiber in the mine. A special monitoring server is set on the ground for data display and storage. At the same time, it can realize remote access of data and facilitate analysis by technicians, as shown in Figure 5.

*4.2. Field Measurement Arrangement of Narrow Barrier Pillar.* In order to verify whether the narrow coal pillar meets the production demand of 4302 working face, surrounding rock deformation monitoring, coal pillar air leakage test, and fire prevention effect inspection are planned to be carried out in the tailentry of 4302 working face. The filed monitoring scheme is shown in Figure 7.

The surrounding rock displacement observation points are arranged in 4302 tailentry. The cross method is used to monitor the displacement of rib-to-rib and roof-to-floor. The observation is performed once a day, and the monitoring period is 50 days.

The air leakage test of coal pillar adopts the method of releasing SF6 tracer gas at fixed point and constant quantity. The release point is located at 50 m away from the setup room in the tailentry. Set 1#-5# gas sample collection points

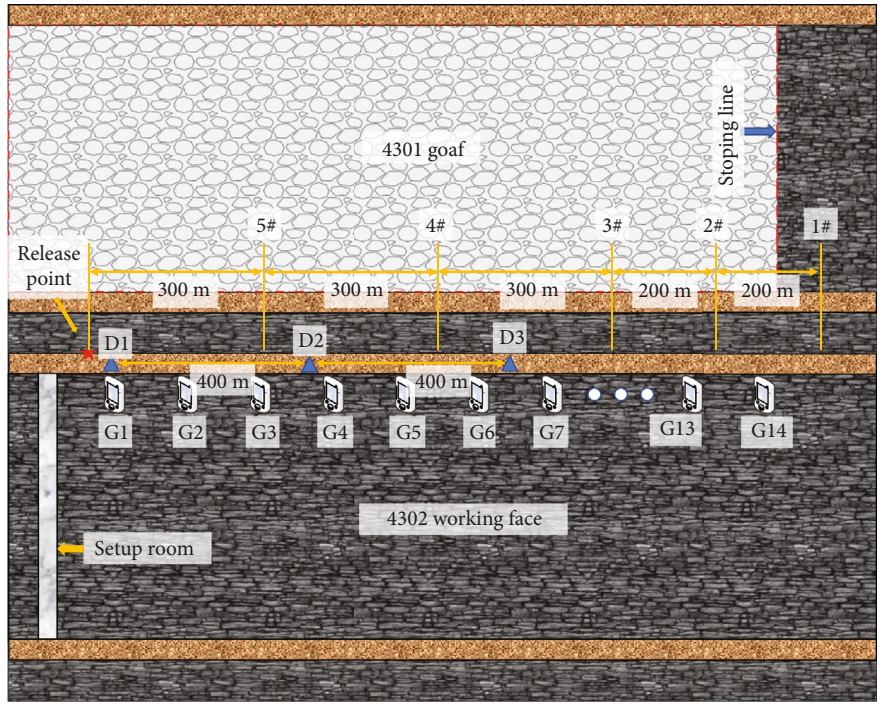


Figure 7: Site layout of coal pillar air leakage and oxidation monitoring.

at 1300 m, 1100 m, 900 m, 600 m, and 300 m from the release point, respectively. The gas sample is collected by manual sampling. The sampling adopts a stainless-steel suction cylinder. The sampling bag adopts a polyethylene plastic bag. The needle and polyethylene tape are used as auxiliary devices for gas collection. During the test, the entry air volume is 1035 $m^3$/min, the tracer gas release is 10 ml/min, and the continuous release is 150 min. In order to eliminate the influence of the unstable stage of initial release, the constant tracer gas collected at the sampling point 20 minutes after release is used as the effective acquisition data. The gas sample is analyzed by SP-3420 gas chromatograph. The instrument has high detection accuracy and can detect tracer gas with concentration of $10^{-12}$. Taking the mean value of collection points as the volume fraction of tracer gas, the air leakage of coal pillar can be calculated according to the following equation:

$$\Delta Q_k = \frac{Q(C_i - C_j)}{C_j}, \tag{18}$$

where $\Delta Q_k$ is the air leakage rate of the coal pillar in the measurement section $K$, $m^3$/min. $Q$ is the ventilation air flow in the entry, $m^3$/min. $C_i$ and $C_j$ are the tracer gas volume fractions at the upper and lower wind sides of the wind flow at the measurement section $K$, respectively.

Early detection of CSC is to collect the symptom information of coal in the initial stage and spontaneous combustion process and judge the change characteristics of CSC state with the help of technical methods and means according to the detected parameters. The schematic diagram of the detection device is shown in Figure 8. In order to determine whether spontaneous combustion of 4302 tailentry coal pillar is induced by pressure crushing during mining, 14 detection points are arranged at equal intervals in the coal pillar to monitor the variation characteristics of temperature, gas composition, and gas volume fraction in the coal pillar with time.

## 5. Results

*5.1. Distribution Characteristics of Side Abutment Pressure.* The monitoring starts from 90 m from the measuring station to the working face. After 50 days of continuous monitoring, the working face pushes 80 m past the measuring station. Figure 9 is the variation curve of borehole stress in coal at different depths of coal wall in tailentry of 4301 working face. It can be seen from Figure 9 that during the process of advancing forward, the mining-induced stress at the 1# measuring point has been less than the primary rock stress and decreased slowly, which indicates that the coal here has been in a state of complete plastic failure under the influence of previous entry excavation without being affected by mining and has lost its most of the bearing capacity. The mining-induced stress at 2# measuring point increases slightly when the working face advances to 50 m away from the measuring station, but the increase is small and then decreases gradually. This indicates that the coal body here enters the yield state and the stress begins to transfer to the deep part of the coal seam. When the working face advances to about 30 m in front of the measuring station, the mining-induced stress at 3# measuring point begins to increase and gradually decreases after a period of time, which indicates that the coal at 3# measuring point also enters the yield state. At this time, the side abutment

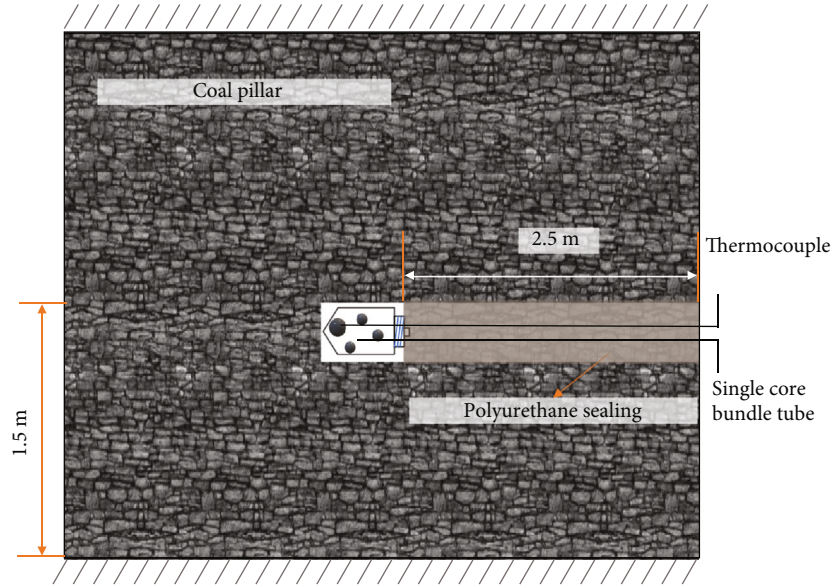


Figure 8: Schematic diagram of coal pillar spontaneous combustion detection device.

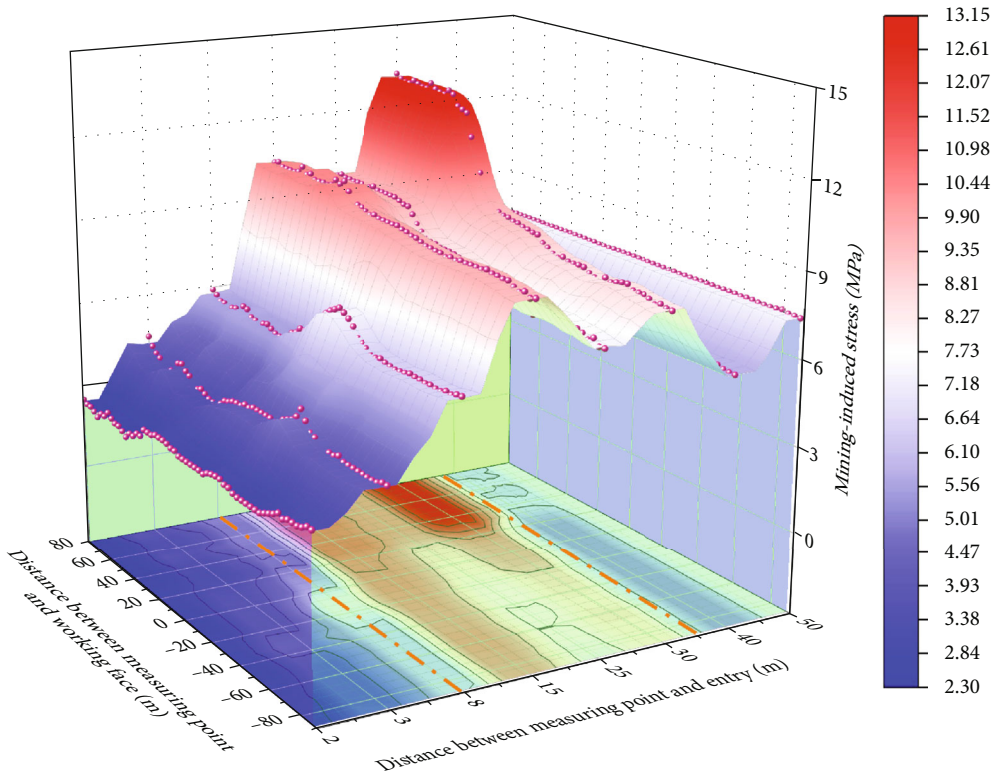


Figure 9: The mining-induced stress data of the borehole at the measuring point in the coal pillar.

pressure continues to transfer to the deep part of the coal seam. When the working face advances to about 20 m in front of the measuring station, the mining-induced stress at 4# and 5# measuring points increases at the same time, indicating that both 4# and 5# measuring points have entered the influence area of side abutment pressure. When the working face is advanced to about 25 m behind the side abutment pressure measuring station, the mining-induced stress at 4# measuring point decreases, while the mining-induced stress at 5# measuring point continues to increase, and the mining-induced stress at 6# measuring point increases sharply. This shows that the high roof breaks, rotates, and sinks at the 4# measuring point and is hinged with the deeper adjacent roof, resulting in a significant

increase in mining-induced stress at the 6# measuring point. Then, the mining-induced stress at 7# measuring point also increases, but the increase range is small, indicating that the peak position of side abutment pressure is about 30 m away from the coal wall of 4301 tailentry. During the whole advancing process of the working face, the mining-induced stress at the 8# measuring point has not changed significantly, indicating that the influence range of side abutment pressure is within 50 m. In addition, after the working face is advanced over 50 m, the mining-induced stress at each measuring point still fluctuates, indicating that at this time, after the fracture of the high roof, there is a local rotary subsidence phenomenon. When the working face is pushed over about 70 m, the mining-induced stress at each measuring point does not change, indicating that the overlying roof slate layer basically tends to be temporarily stable.

*5.2. Calculation Results of Narrow Coal Pillar Theoretical Model.* It can be seen from Equation (15) that the instability of coal pillar in gob-side entry is related to the stiffness of plastic failure area and the stiffness ratio of stable elastic core area. And it is related to density of overlying strata, physical and mechanical parameters of coal pillar, dip angle of coal seam and weak face, and buried depth and mining width of working face.

According to the coal pillar instability criterion of cusp catastrophe theory, the relevant parameters of surrounding rock of 4302 working face are substituted into Equation (15). The instability condition of barrier pillar in 4302 working face is as follows: the width of coal pillar $a \leq 6.8$ m, so the width of barrier pillar shall not be less than 6.8 m.

Equation (17) shows that the minimum width of barrier pillar is directly proportional to its permeability characteristics and air leakage pressure difference. The greater the permeability coefficient of coal pillar, the wider the width of coal pillar required to prevent CSC. The measured wind pressures inside and outside the closed wall of 4301 headentry are 78941 Pa and 78896 Pa, respectively. Therefore, after the construction of 4302 tailentry is completed, the gas pressure difference on both sides of the coal pillar is about 45 Pa. The original permeability of the coal pillar of the adjacent 4301 headentry is 0.15 $m^2$. Considering the most unfavorable factors of fire prevention, the permeability of the coal pillar after mining is taken as 6 times the original permeability. According to Equation (17), the width of the barrier pillar of 4302 tailentry shall be greater than 6.75 m.

Based on the monitoring results of Section 5.1, under the principle of maintaining the stability of the entry, combined with the actual production on site, the width of the barrier pillar of the 4302 tailentry is determined to be 7 m.

### 5.3. Field Measurement of Barrier Pillar

*5.3.1. Deformation Monitoring of Surrounding Rock.* The entry developed along the gob of 4301 working face according to the width of 7 m coal pillar in the filed construction. Three observation stations set at the head after 60 m, 460 m, and 860 m excavation from setup room. Figure 10 shows the observation results of the approaching amount of rib-to-rib and roof-to-floor of the 4302 tailentry. At the initial stage of monitoring, the rate of deformation of surrounding rock was not high. After the third day, the deformation entered an accelerated state. When the monitoring progressed to the 13th day, the surrounding rock deformed into an inflection point, and the deformation rate dropped sharply. At this time, the deformation of the roof-to-floor is 25 mm, and the distance between the rib-to-rib is 480 mm. From the 13th day to the 37th day, the surrounding rock displacement tended to be stable, the maximum moving distance of the rib-to-rib reached 520 mm, and the maximum moving distance of the roof-to-floor reached 280 mm. Compared with the width and height of the entry, the deformation is in a controllable range. This shows that the 7 m wide section coal pillar can meet the stability requirements of the surrounding rock of the entry.

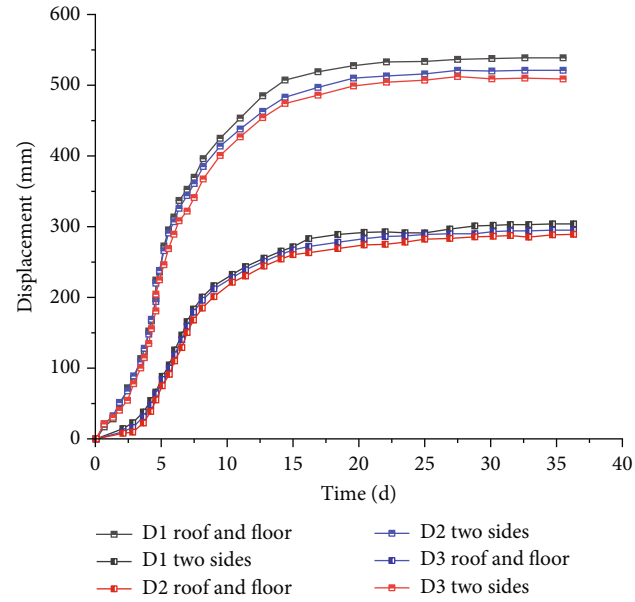


Figure 10: Deformation of surrounding rock in 4302 tailentry.

*5.3.2. Fire Prevention Test for 4302 Barrier Pillar.* Since the monitoring points are set to follow the excavation of the 4302 tailentry, the monitoring data of each monitoring point are the whole process of entry excavation, setup room penetration, and mining of the working face. The volume fraction of tracer gas is shown in Figure 11. The maximum air leakage between measuring points 1# and 2# is 12.67 $m^3$/min, and the minimum 2# and 3# is only about 1.21 $m^3$/min, of which the air leakage between 3# and 4# measuring points is 5.38 $m^3$/min. The total air leakage of coal pillar is 23.74 $m^3$/min, and the 7 m coal pillar reserved in 4302 tailentry effectively realizes the function of blocking air leakage.

The monitoring results of spontaneous combustion detection device in coal pillar show that the temperature difference between entry and coal pillar is always maintained within 1.5°C, and there is no increase. On the 21st and 52nd day of monitoring, G4 station detected that the volume fraction of carbon monoxide was $1.57 \times 10^{-6}$ and $0.83 \times 10^{-6}$, and there is no other sign gas. The volume fraction of carbon monoxide on the 22nd and 53rd days was 2.08

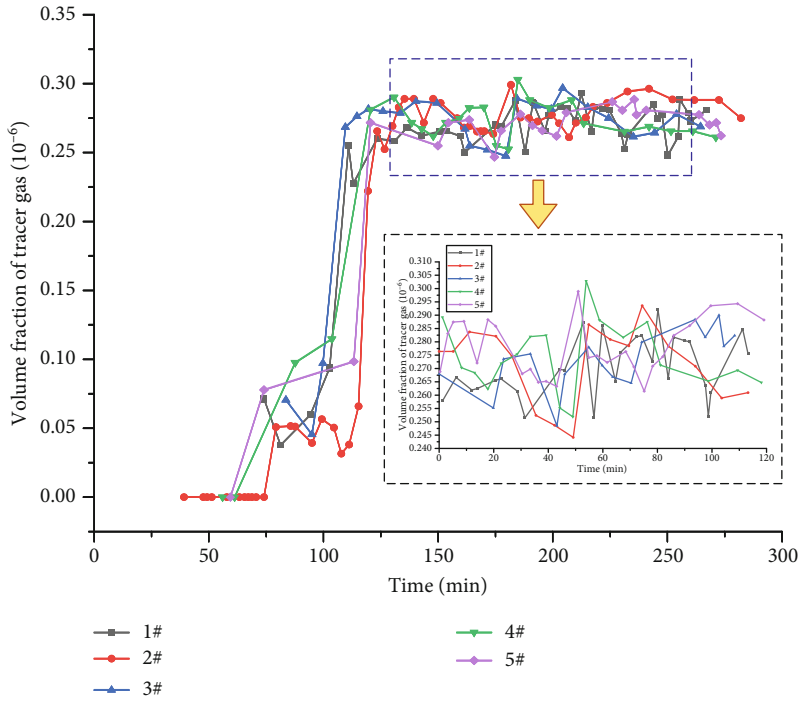


Figure 11: Tracer gas volume fraction in the 4302 tailentry.

$\times 10^{-6}$ and $1.41 \times 10^{-6}$ at G5 station, and no other gas is detected. In addition, the gas inside each test borehole is normal. Therefore, there is no sign of spontaneous combustion in the whole process of narrow coal pillar in 4302 tailentry section. It can be considered that 7 m coal pillar can meet the air leakage prevention requirements of spontaneous combustion coal seam under the influence of mining.

## 6. Conclusions

In order to obtain the optimal width of coal pillar in gob-side entry of LTCC working face in spontaneous combustion coal seam, take the 4302 tailentry of Changheng Mine as the engineering background. The characteristics of rock mass collapse and mining-induced stress redistribution in the around area of coal pillar were analyzed. The cusp catastrophe model for sudden instability of coal pillar and the limit width model of coal pillar spontaneous combustion due to air leakage were established. Furthermore, the side abutment pressure of coal pillar in the adjacent 4301 working face was monitored. Through the filed measurement, the deformation of entry surrounding rock and the fire prevention effect of coal pillar were monitored. The conclusions are as follows:

(1) By analyzing the characteristics of rock mass collapse and mining-induced stress distribution in the area around the coal pillar, the reasonable location of the coal pillar was determined. The criterion of cusp catastrophe model for sudden instability of coal pillar was obtained, and the limit relationship between pillar width and spontaneous combustion caused by air leakage was determined, which lays a foundation for determining the retention optimization scheme of coal pillar along the 4302 tailentry

(2) Using the method of monitoring side abutment pressure in the drainage entry, the distribution of side abutment pressure in the LTCC process of 4301 working face was measured reasonably and accurately. The field measured data showed that 2-8 m was the stress-relaxation area of side solid coal. The cusp catastrophe model of the coal pillar along the gob-side entry shows that the instability of the coal pillar is related to the stiffness of the plastic failure area and the stiffness ratio of the stable elastic core area. And it is related to density of overlying strata, physical and mechanical parameters of coal pillar, dip angle of coal seam and weak face, and buried depth and mining width of working face. When the coal pillar width $a \leq 6.8$ m, the coal pillar in 4302 working face will be unstable. It is comprehensively determined that the reasonable reserved width of coal pillar is 7 m

(3) The displacement monitoring after entry completion shows that the maximum displacement of rib-to-rib of 4302 tailentry was 520 mm, and the maximum displacement of roof-to-floor was 280 mm, which meets the stability requirements of tailentry surrounding rock. A total of 14 CSC observation stations were arranged at equal intervals in the coal pillar. The monitoring results showed that the carbon monoxide volume fraction was in the normal range during the entire process of entry excavation, setup room, and normal mining, and no other signs

of gas were found. It shows that the coal pillar in the 7 m section meets the air leakage prevention requirements of the spontaneous combustion coal seam, and no oxidation spontaneous combustion phenomenon occurs

## Data Availability

The data used for conducting classifications are available from the corresponding author upon request.

## Conflicts of Interest

The authors declared no potential conflicts of interest with respect to the research, authorship, and publication of this article.

## Authors' Contributions

All authors contributed to this paper. Qiang Fu prepared and edited the manuscript. Qinjie Liu and Ke Yang made a substantial contribution to the data analysis and revised the article. Shuai Liu and Xin Lyu reviewed the manuscript and processed the investigation during the research process. Ke Yang, Qinjie Liu, and Qiang Fu provided fund support.

## Acknowledgments

This work is supported by the Institute of Energy, Hefei Comprehensive National Science Center under Grant (No. 19KZS203 and No. 21KZS215), the Natural Science Foundation of Anhui Province (1708085ME133), and the Graduate Innovation Fund Project of Anhui University of Science and Technology of China (2020CX1002).

## References

[1] J. Wang, Z. Wang, and Y. Li, "Longwall top coal caving mechanisms in the fractured thick coal seam," *International Journal of Geomechanics*, vol. 20, no. 8, article 06020017, 2020.

[2] Z. Song, C. Kuenzer, H. Zhu et al., "Analysis of coal fire dynamics in the Wuda syncline impacted by fire-fighting activities based on in-situ observations and Landsat-8 remote sensing data," *International Journal of Coal Geology*, vol. 141-142, pp. 91–102, 2015.

[3] D. Wei, C. Du, B. Lei, and Y. Lin, "Prediction and prevention of spontaneous combustion of coal from goafs in workface: a case study," *Case Studies in Thermal Engineering*, vol. 21, article 100668, 2020.

[4] M. Shabanimashcool and C. C. Li, "A numerical study of stress changes in barrier pillars and a border area in a longwall coal mine," *International Journal of Coal Geology*, vol. 106, pp. 39–47, 2013.

[5] Y. L. Tan, F. H. Yu, J. G. Ning, and T. B. Zhao, "Design and construction of entry retaining wall along a gob side under hard roof stratum," *International Journal of Rock Mechanics and Mining Sciences*, vol. 77, pp. 115–121, 2015.

[6] Z. Zhang, J. Bai, Y. Chen, and S. Yan, "An innovative approach for gob-side entry retaining in highly gassy fully- mechanized longwall top-coal caving," *International Journal of Rock Mechanics and Mining Sciences*, vol. 80, pp. 1–11, 2015.

[7] S. Yan, J. Bai, X. Wang, and L. Huo, "An innovative approach for gateroad layout in highly gassy longwall top coal caving," *International Journal of Rock Mechanics and Mining Sciences*, vol. 59, no. 4, pp. 33–41, 2013.

[8] S. Yan, T. X. Liu, J. B. Bai, and W. D. Wu, "Key parameters of gob-side entry retaining in a gassy and thin coal seam with hard roof," *Processes*, vol. 6, no. 5, pp. 51–65, 2018.

[9] Z. T. Bieniawski, "The effect of specimen size on compressive strength of coal," *International Journal of Rock Mechanics and Mining Sciences and Geomechanics Abstracts*, vol. 5, no. 4, pp. 325–335, 1968.

[10] M. Salamon and A. H. Munro, "A study of the strength of coal pillars," *Journal of the South African Institute of Mining and Metallurgy*, vol. 68, no. 2, pp. 55–67, 1967.

[11] R. Bertuzzi, K. Douglas, and G. Mostyn, "An approach to model the strength of coal pillars," *International Journal of Rock Mechanics and Mining Sciences*, vol. 89, pp. 165–175, 2016.

[12] G. S. Esterhuizen, D. F. Gearhart, and I. B. Tulu, "Analysis of monitored ground support and rock mass response in a longwall tailgate entry," *International Journal of Mining Science and Technology*, vol. 28, no. 1, pp. 43–51, 2018.

[13] S. J. Chen, H. L. Wang, H. Y. Wang, W. J. Guo, and X. S. Li, "Strip coal pillar design based on estimated surface subsidence in eastern China," *Rock Mechanics and Rock Engineering*, vol. 49, no. 9, pp. 3829–3838, 2016.

[14] B. Yu, Z. Zhang, T. Kuang, and J. Liu, "Stress changes and deformation monitoring of longwall coal pillars located in weak ground," *Rock Mechanics and Rock Engineering*, vol. 49, no. 8, pp. 3293–3305, 2016.

[15] L. Jiang, A. Sainoki, H. S. Mitri, N. Ma, H. Liu, and Z. Hao, "Influence of fracture-induced weakening on coal mine gateroad stability," *International Journal of Rock Mechanics and Mining Sciences*, vol. 88, pp. 307–317, 2016.

[16] Z. Zhou, Y. Zhao, W. Cao, L. Chen, and J. Zhou, "Dynamic response of pillar workings induced by sudden pillar recovery," *Rock Mechanics and Rock Engineering*, vol. 51, no. 10, pp. 3075–3090, 2018.

[17] G. C. Zhang, F. L. He, H. G. Jia, and Y. H. Lai, "Analysis of gateroad stability in relation to yield pillar size: a case study," *Rock Mechanics and Rock Engineering*, vol. 50, no. 5, pp. 1263–1278, 2017.

[18] Q. Xu, J. B. Bai, S. Yan, R. Wang, S. Wu, and T. X. Chu, "Numerical study on soft coal pillar stability in an island longwall panel," *Advances in Civil Engineering*, vol. 2021, Article ID 8831778, 13 pages, 2021.

[19] H. Wu, X. Wang, W. Wang, G. Peng, and Z. Zhang, "Deformation characteristics and mechanism of deep subsize coal pillar of the tilted stratum," *Energy Science and Engineering*, vol. 8, no. 2, pp. 544–561, 2020.

[20] Y. Liu, H. Wen, J. Guo, Y. Jin, G. Wei, and Z. Yang, "Coal spontaneous combustion and $N_2$ suppression in triple goafs: a numerical simulation and experimental study," *Fuel*, vol. 271, article 117625, 2020.

[21] P. Hou, X. Liang, Y. Zhang, J. He, F. Gao, and J. Liu, "3D multiscale reconstruction of fractured shale and influence of fracture morphology on shale gas flow," *Natural Resources Research*, vol. 30, no. 3, pp. 2463–2481, 2021.

[22] J. B. Bai, W. L. Shen, G. L. Guo, X. Y. Wang, and Y. Yu, "Roof deformation, failure characteristics, and preventive techniques of gob-side entry driving heading adjacent to the advancing

working face," *Rock Mechanics and Rock Engineering*, vol. 48, no. 6, pp. 2447–2458, 2015.

[23] X. Liang, P. Hou, Y. Xue, X. Yang, F. Gao, and J. Liu, "A fractal perspective on fracture initiation and propagation of reservoir rocks under water and nitrogen fracturing," *Fractals*, 2021.

[24] H. Zhang, Z. Wan, Z. Ma, and Y. Zhang, "Stability control of narrow coal pillars in gob-side entry driving for the LTCC with unstable overlying strata: a case study," *Arabian Journal of Geosciences*, vol. 11, no. 21, 2018.

[25] X. Wang, K. Guan, T. Yang, and X. Liu, "Instability mechanism of pillar burst in asymmetric mining based on cusp catastrophe model," *Rock Mechanics and Rock Engineering*, vol. 54, no. 3, pp. 1463–1479, 2021.

[26] Z. P. Meng, P. Zhang, and Y. D. Tian, "Experimental analysis of stress-strain, permeability and acoustic emission of coal reservoir under different confining pressures," *Journal of China Coal Society*, vol. 45, no. 7, pp. 2544–2551, 2020.

[27] F. Wang, C. Zhang, and N. Liang, "Gas permeability evolution mechanism and comprehensive gas drainage technology for thin coal seam mining," *Energies*, vol. 10, no. 9, p. 1382, 2017.

[28] P. Hou, X. Liang, F. Gao, J. B. Dong, J. He, and Y. Xue, "Quantitative visualization and characteristics of gas flow in 3D pore-fracture system of tight rock based on Lattice Boltzmann simulation," *Journal of Natural Gas Science and Engineering*, vol. 89, article 103867, 2021.

[29] Q. L. Zuo, J. S. Li, and Y. J. Wang, "Distribution law for the danger area for spontaneous coal combustion in a dynamic goaf with low air leakage speed," *Thermal Science*, vol. 25, no. 5 Part A, pp. 3229–3237, 2021.

[30] Q. Wang, M. He, S. Li et al., "Comparative study of model tests on automatically formed roadway and gob-side entry driving in deep coal mines," *International Journal of Mining Science and Technology*, vol. 31, no. 4, pp. 591–601, 2021.

[31] Q. Wang, H. Gao, B. Jiang et al., "Research on reasonable coal pillar width of roadway driven along goaf in deep mine," *Arabian Journal of Geosciences*, vol. 10, no. 21, 2017.

[32] State Administration of Work Safety, *Coal Mine Safety Regulations*, China Coal Industry Publishing House, Beijing, 2016.